Thermally Generated Spin Signals in a Nondegenerate Silicon Spin Valve

Naoto Yamashita,[1,†] Yuichiro Ando,[1,†] Hayato Koike,[2] Shinji Miwa,[3] Yoshishige Suzuki,[3] and Masashi Shiraishi[1,†,*]

[1]*Department of Electronic Science and Engineering, Kyoto University, Kyoto 615-8510, Japan*
[2]*Technology HQ, TDK Corporation, Chiba 272-8558, Japan*
[3]*Graduate School of Engineering Science, Osaka University, Toyonaka 560-8531, Japan*

(Received 13 July 2017; revised manuscript received 20 February 2018; published 2 May 2018)

Thermally generated spin signals are observed in a nondegenerate Si spin valve. The spin-dependent Seebeck effect is used for thermal spin-signal generation. A thermal gradient of about 200 mK at the interface of Fe and Si enables the generation of a spin voltage of 8 μV at room temperature. A simple expansion of the conventional spin-drift-diffusion model that takes into account the spin-dependent Seebeck effect shows that semiconductor materials are more promising for thermal spin-signal generation comparing than metallic materials, and thus enable efficient heat recycling in semiconductor spin devices.

DOI: 10.1103/PhysRevApplied.9.054002

I. INTRODUCTION

Spin caloritronics, which combines spintronics and thermoelectricity [1], is a new field of spintronics that is attracting great attention. In spintronics, spin currents, such as pure spin currents and spin-polarized currents, are used to propagate information. While spin currents have been generated electrically and dynamically in a wide variety of materials [2–10], the utilization of heat currents to generate spin currents is a new method that has spawned the field of spin caloritronics [11–19]. The coupling of spin current and heat current leads novel physical phenomena, with a number of attractive caloritronic effects such as the spin-Seebeck effect [13,14], the spin-dependent Seebeck effect [15], and the spin-Peltier effect [11,16]. However, such spin-caloritronic effects have been limited to metals [15,16,18,19] and magnetic insulators [14]; the methodology has not yet been widely extended to semiconductors. One noteworthy example of a spin-caloritronic effect in semiconductor is the Seebeck spin tunneling [20], where the controversial three-terminal method (only one ferromagnetic electrode is used to observe the Hanle-like signals) [21] was used and thermal spin accumulation (not spin transport) was claimed. However, the reliability of the three-terminal method has been under strong debate [22–29]. Thus, it is worth realizing spin transport in semiconductors by using spin-caloritronic effects. Because the spin-Seebeck effect is manifested only in a ferrimagnetic insulator, the spin-dependent Seebeck effect is a strong candidate for achieving thermally induced spin injection and transport in semiconductors.

In the present study, we achieve a spin-caloritronic effect, namely, thermal spin-signal generation in nondegenerate Si, the most common material in semiconductor electronics, by utilizing the spin-dependent Seebeck effect. The thermal gradient generated by electric current injection, at the interface between a ferromagnetic electrode and a nondegenerate Si spin channel, enables the generation of a spin current in the Si. A simple expansion of the conventional spin-drift-diffusion model that takes into account the spin-dependent Seebeck contribution shows that, under the same thermal gradient, a semiconductor is likely to generate larger thermal spin signals than a metal.

II. EXPERIMENTS

A nondegenerate phosphorus (P)-doped ($n \approx 2 \times 10^{18}$ cm^{-3}) silicon spin valve is fabricated on a silicon-on-insulator (SOI) substrate with the structure of Si(100 nm)/SiO_2(200 nm)/bulk Si [see Fig. 1(a)], which is the same as the structure of a spin MOSFET. The conductivity of the Si channel is measured by using a four-probe method. The upper Si layer is P doped by ion implantation. Ferromagnetic tunnel junctions are formed on silicon with a higher doping level (n^+-Si; $t = 20$ nm; $n \approx 5 \times 10^{19}$ cm^{-3}) by using an 0.8-nm-thick MgO tunnel barrier and 17-nm-thick Fe thin film. After the native oxide layer on the Si channel is removed using an HF solution, Pd(3 nm)/Fe(13 nm)/MgO(0.8 nm) is grown on the etched surface by molecular beam epitaxy. The role of the MgO tunneling barrier is to avoid the conductance mismatch problem, which becomes obvious also in thermal spin injection into semiconductors (discussed later, but already pointed out in Ref. [15]), in addition to in electric spin injection [30], and the barrier is indispensable in this experiment. Nonlinearity in a current-voltage (I-V) curve appears due to the MgO barrier, and an

*Corresponding author.
mshiraishi@kuee.kyoto-u.ac.jp
†These authors contributed equally to this work.

 © 2018 American Physical Society

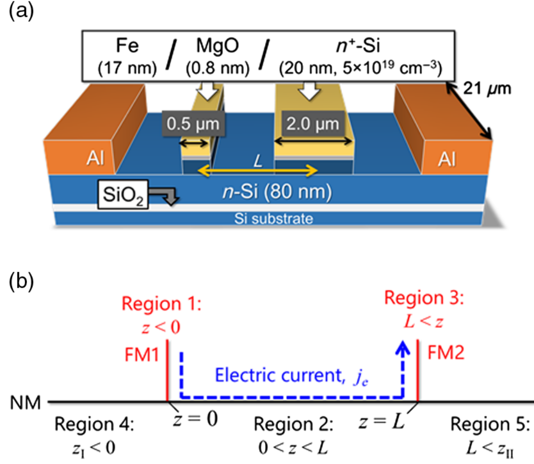

FIG. 1. (a) Nondegenerate ($n \approx 2 \times 10^{18}$ cm^{-3}) Si spin valves are fabricated on a silicon-on-insulator (SOI) substrate. The ferromagnetic tunnel junctions are formed on n^+-Si (20-nm thick with a doping concentration of 5×10^{19} cm^{-3}) using an MgO tunnel barrier (0.8-nm thick) and 17-nm-thick Fe thin film. After nanofabrication of the two ferromagnetic electrodes, the center-to-center length L is 1.75 μm. (b) A schematic illustration of our device to calculate the magnitude of thermal spin signals. In this model, the device is divided in five regions: the red and black regions are ferromagnetic (FM) and nonmagnetic (NM), respectively. An electric current flows from FM1 to FM2, i.e., spins are injected from FM2. We adopt an open-circuit condition for the calculation. For more detail, see Sec. A of the Supplemental Material in Ref. [31].

alternative approach for an investigation of physics in the thermal spin injection into semiconductors is established. The establishment of the approach is also significant to solve a problem of nonlinear bias voltage dependence of a spin signal appearing in most of spin devices, which is also discussed later. We etched out Pd(3 nm)/Fe(3 nm) layers, and Ta (3 nm) is grown on the remaining Fe. The two contacts are 0.5×21 μm^2 and 2×21 μm^2, respectively. The Si channel surface and sidewalls at the ferromagnetic contacts are buried under SiO_2. The nonmagnetic electrodes (21×21 μm^2) are made of Al and produced by ion milling. The center-to-center distance between the ferromagnet (FM) electrodes L is set to 1.75 μm. The spin-valve characteristics are determined by using a probing station (Janis Research Company Inc., ST-500), a source meter (Keithley Instruments, 2400 and 2401), and a digital multimeter (Keithley Instruments, 2010). Thermal spin signals are detected through an ac lock-in technique, in which the ac frequency is applied using a LI5655 lock-in amplifier (NF Corporation). All measurements are performed at RT.

To detect thermal and electrical spin signals in Si, we use an electrical local three-terminal-magnetoresistance (3T-MR) method [32,33]. It is worth noting that this method is different from the controversial three-terminal method [21]. We use two ferromagnetic electrodes and measure the magnetoresistance in addition to Hanle-type spin-precession signals, which provide strong evidence for successful spin injection and transport in Si [32,33]. The other advantage of the present method is that, owing to spin drift, it yields larger spin signals than the nonlocal four-terminal method, where only spin diffusion contributes to spin transport [33].

Because the thermal spin signal due to the spin-dependent Seebeck effect scales with the Joule heating, we use an ac lock-in technique to measure the thermally induced signals, as was already established in the previous study [15]. The ac frequency is set to 17 Hz to avoid unnecessary thermal contribution to the experiment [15,17]. In fact, the previous study [17] used the similar experimental condition ($f < 20$ Hz). Such low frequency does not affect the spin relaxation time because the time scales are largely different. The total output voltage due to spin accumulation (electrically and thermally), $V_{\rm detect}$, as a function of the injected current I is given by $V_{\rm detect} = R_1 I + R_2 I^2 + \cdots$, where R_1 and R_2 are parameters pertaining to the electrically generated spin signal and the thermal spin signal, respectively. We measure the second-harmonic term $R_2 I^2$ linked to the thermal spin signal by using the ac lock-in technique. A precise estimation of thermal spin-signal components may not be possible using the ac lock-in measurement scheme owing to a number of factors The MgO tunneling barrier induces nonlinearity in I-V characteristics, which generates spurious components in the second-harmonic signals. The nonlinear bias dependence of spin signals [34] also contributes to the generation of spurious second-harmonic signals in the ac lock-in technique. However, as described below, particular attention is paid to eliminate these spurious effects in our study.

III. RESULTS AND DISCUSSION

Figures 2(a) and 2(b) show the measurement setup and the thermally induced magnetoresistance observed in nondegenerate Si, respectively. The dc and ac bias voltages are set to 3.0 and 1.0 V root-mean-square (rms), respectively. As can be seen in Fig. 2(b), a second-harmonic voltage, $R_2 I^2$, of 19 μV is measured, including the thermal spin signal and the spurious signals, described in the previous section. On the basis of Fourier transformation analysis using the I-V curve and the bias dependence of electric spin signals, which is described later, the contribution of the spurious effects is estimated to be 10.7 μV for an ac injection bias of 1.0 V. Figure 2(c) shows the thermal spin signals as a function of the square of the ac electric current after removal of spurious signals. As predicted by theory, our experimental results exhibit clear I^2 dependence. This provides evidence that the second-harmonic voltage can be attributed to the thermal gradient at the interface of Fe and Si via MgO.

In order to estimate the thermal gradient in our device, a model is constructed by combining the conventional spin drift-diffusion model and the spin-dependent Seebeck

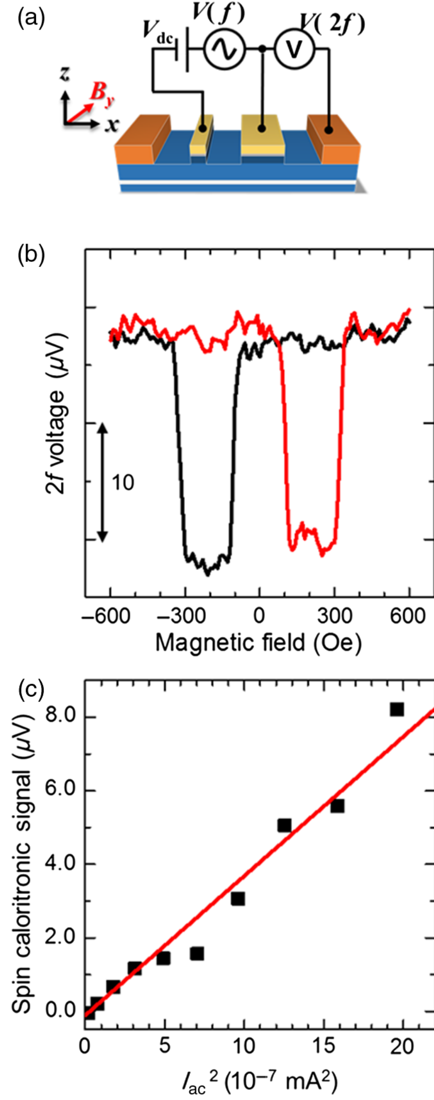

FIG. 2. (a) A scheme of measuring thermal spin signals from the nondegenerate Si spin valves. The ac lock-in technique is used to detect the second-harmonic ($2f$) spin signals attributed to the spin-dependent Seebeck effect. (b) A $2f$ spin signal observed from the Si spin valve at RT. The external magnetic field is swept from negative to positive (the red solid line) and from positive to negative (the blue solid line), and a $2f$ voltage of 19 μV is observed. The offset voltage is measured to be 5.86 mV. Note that spurious signals in addition to the thermal spin signal are included in this $2f$ signal. (c) I_{ac}^2 dependence of the thermal spin signals. The detail of discriminating the thermal spin signals and spurious signals is described in the main text. The black closed squares are experimental results and the red solid line shows the fitting line. The experimental results are well fit.

effects. Since a bias electric field is applied to the Si spin channel, the upstream and downstream spin-transport length scales (λ_u and λ_d) are used instead of the spin-diffusion length of Si (λ_N), where $\lambda_{u(d)} = [+(-)(|eE|/2k_BT)+\sqrt{(eE/2k_BT)^2+(1/\lambda_N)^2}]^{-1}$ (E is the electric field in the spin channel, and k_B is the Boltzmann constant) [31]. Furthermore, terms due to the spin-dependent Seebeck effect are included in the description of up- and down-spin currents: $j_s = -\sigma_s[(\partial V_s/\partial z) + S_s\nabla T]$, $(s = \uparrow, \downarrow)$ [15], where j_s is the spin current, σ_s is the conductivity, z is a position coordinate, V_s is the spin-dependent voltage [$V_s = \mu_s/e$, $e < 0$; e (<0) is the electric charge and μ_s is the electrochemical potential], $S_\uparrow$ and $S_\downarrow$ are the Seebeck coefficient of up and down spins of Fe, respectively, and T is the temperature. This model takes into account the following: (i) the device structure with a contribution from the spin-dependent interface tunnel resistance due to the MgO (the thickness of the MgO is neglected), (ii) the back flow of the spin current from FM2, and (iii) the spin-drift effect due to electrical current injection into Si (see also Ref. [33]). Figure 1(b) shows positional coordinates, along with a schematic of the device structure [ferromagnet 1 (FM1); nonmagnet (NM); ferromagnet 2 (FM2)] under the $3T$-MR measurement scheme used in the modeling. The electric current flows from FM1 to FM2; i.e., spins (electrons) are injected from FM2. The spin-dependent voltages and spin currents for the up and down spins in FM1 and FM2 under the parallel magnetization configuration and the assumption that the thermal gradient exists only at $z = L$ (the spin and the charge injector side) are described as

$$V_{1,\uparrow(\downarrow)} = -\frac{j_e}{\sigma_F}z + (-)V_1^-\frac{\sigma_{\downarrow(\uparrow)1}}{\sigma_F}\exp\left(\frac{z}{\lambda_F}\right) + D,$$

$$j_{1,\uparrow(\downarrow)} = \frac{\sigma_{\uparrow(\downarrow)1}}{\sigma_F}j_e - (+)\frac{V_1^-}{R_F}\exp\left(\frac{z}{\lambda_F}\right) - \sigma_{\uparrow(\downarrow)1}S_{\uparrow(\downarrow)1}\nabla T_0, \quad \text{(FM, region 1)} \tag{1}$$

$$V_{3,\uparrow(\downarrow)} = -\frac{j_e}{\sigma_F}(z-L) - \frac{j_e}{\sigma_N}L + (-)V_3^+\frac{\sigma_{\downarrow(\uparrow)3}}{\sigma_F} \times \exp\left(-\frac{z-L}{\lambda_F}\right) - E,$$

$$j_{3,\uparrow(\downarrow)} = \frac{\sigma_{\downarrow(\uparrow)3}}{\sigma_F}j_e + (-)\frac{V_3^+}{R_F}\exp\left(-\frac{z_{II}-L}{\lambda_F}\right) - \sigma_{\uparrow(\downarrow)3}S_{\uparrow(\downarrow)3}\nabla T_L, \quad \text{(FM, region 3)} \tag{2}$$

where, $j_e, \lambda_F, R_F, \sigma_{Fi}, D, E$, and L are the electric current, the spin-diffusion length of FM, the spin resistance of FM [defined as $R_F = \lambda_F(\sigma_\uparrow{}^{-1} + \sigma_\downarrow{}^{-1})$], the conductivity of FM "$i(=1,3)$" $(=\sigma_{\uparrow i} + \sigma_{\downarrow i})$, the spin-accumulation voltage at the interface between FM1 and NM, that between FM2 and NM, and the gap length between FM1 and FM2, respectively. ∇T_0 and ∇T_L are the temperature gradients at the point of $z = 0$ and $z = L$. V_1^- and V_3^+ are the spin-dependent voltages at FM1 and FM2. Similarly, the spin-dependent voltages in the three NM regions (regions 2, 4, and 5), including the spin-drift effect discussed above, are written as

$$V_{2,\uparrow(\downarrow)} = +(-)\frac{V_2^+}{2}\exp\left(-\frac{z}{\lambda_u}\right) + (-)\frac{V_2^-}{2}\exp\left(\frac{z-L}{\lambda_d}\right) - \frac{j_e}{\sigma_N}z,$$
$$j_{2,\uparrow(\downarrow)} = +(-)\frac{V_2^+}{R_u}\exp\left(-\frac{z}{\lambda_u}\right) - (+)\frac{V_2^-}{R_d}\exp\left(\frac{z-L}{\lambda_d}\right) + \frac{j_e}{2} - \frac{1}{2}\sigma_N S_N \nabla T_N, \qquad \text{(NM, region 2)} \tag{3}$$

$$V_{4,\uparrow(\downarrow)} = +(-)\frac{V_4^-}{2}\exp\left(\frac{z_I}{\lambda_N}\right), \quad j_{4,\uparrow(\downarrow)} = -(+)\frac{V_4^-}{R_N}\exp\left(\frac{z_I}{\lambda_d}\right) - \frac{1}{2}\sigma_N S_N \nabla T_N, \qquad \text{(NM, region 4)} \tag{4}$$

$$V_{5,\uparrow(\downarrow)} = -\frac{j_e}{\sigma_N}L + (-)\frac{V_5^+}{2}\exp\left(-\frac{z_{II}-L}{\lambda_N}\right), \quad j_{5,\uparrow(\downarrow)} = +(-)\frac{V_5^+}{R_N}\exp\left(-\frac{z_{II}-L}{\lambda_N}\right) - \frac{1}{2}\sigma_N S_N \nabla T_N, \qquad \text{(NM, region 5)} \tag{5}$$

$$R_{N(d,u)} = \frac{4}{\sigma_N}\lambda_{N(d,u)}, \tag{6}$$

where ∇T_N is the thermal gradient in NM, and $\sigma_0(=2\sigma_N)$ is the conductivity of NM. At $z=0$ and L. The continuity conditions for spin voltage and spin current for up and down spins, including the interfacial spin-dependent tunneling resistance, are set to be

$$V_{1,\uparrow(\downarrow)} - R_{i1\uparrow(\downarrow)}j_{1\uparrow(\downarrow)} = V_{2,\uparrow(\downarrow)} = V_{3,\uparrow(\downarrow)}, \quad j_{1,\uparrow(\downarrow)} = j_{2,\uparrow(\downarrow)} + j_{3,\uparrow(\downarrow)}, \qquad (\text{at } z=0) \tag{7}$$

$$V_{5,\uparrow(\downarrow)} + R_{i3\uparrow(\downarrow)}j_{1\uparrow(\downarrow)} = V_{3,\uparrow(\downarrow)} = V_{4,\uparrow(\downarrow)}, \quad j_{3,\uparrow(\downarrow)} = j_{4,\uparrow(\downarrow)} + j_{5,\uparrow(\downarrow)}, \qquad (\text{at } z=L) \tag{8}$$

where $R_{i1\uparrow(\downarrow)}$ and $R_{i3\uparrow(\downarrow)}$ are the spin-dependent resistance due to the tunneling barrier at the interface between FM1 and NM and that between FM2 and NM, respectively. D in Eq. (1) is the spin-accumulation voltage in the $3T$-MR scheme, which can be described under the parallel magnetization configuration as

$$D^{\text{parallel}} = \left[\frac{1}{2}\alpha_{F1} + (\sigma_{\uparrow1}R_{i1\uparrow} - \sigma_{\downarrow1}R_{i1\downarrow})\frac{q_u}{\sigma_{F1}}\right]V_2^+ + \left[\frac{1}{2}\alpha_{F1} - (\sigma_{\uparrow1}R_{i1\uparrow} - \sigma_{\downarrow1}R_{i1\downarrow})\frac{u_d}{\sigma_{F1}}\right]V_2^-\eta_d + (\sigma_{\uparrow1}R_{i1\uparrow} + \sigma_{\downarrow1}R_{i1\downarrow})\frac{j_e}{2\sigma_{F1}},$$
$$V_2^+ = \frac{[-(Q_d+1)(R_{F1}\alpha_{F1} - R_{i1\uparrow} + R_{i1\downarrow}) + (U_d-1)\eta_d(R_{F3}\alpha_{F3} - R_{i3\uparrow} + R_{i3\downarrow})]}{(U_u-1)(U_d-1)\eta_u\eta_d - (Q_d+1)(Q_u+1)}\frac{j_e}{2}$$
$$-\frac{\eta_d R_{F3}(U_d-1)(\sigma_{\uparrow3}S_\uparrow - \sigma_{\downarrow3}S_\downarrow)}{(U_u-1)(U_d-1)\eta_u\eta_d - (Q_d+1)(Q_u+1)}\frac{\nabla T}{2},$$
$$V_2^- = \frac{[-(U_u-1)\eta_u(R_{F1}\alpha_{F1} - R_{i1\uparrow} + R_{i1\downarrow}) + (Q_u+1)(R_{F3}\alpha_{F3} - R_{i3\uparrow} + R_{i3\downarrow})]}{(U_u-1)(U_d-1)\eta_u\eta_d - (Q_d+1)(Q_u+1)}\frac{j_e}{2}$$
$$-\frac{R_{F3}(Q_u+1)(\sigma_{\uparrow3}S_\uparrow - \sigma_{\downarrow3}S_\downarrow)}{(U_u-1)(U_d-1)\eta_u\eta_d - (Q_d+1)(Q_u+1)}\frac{\nabla T}{2}, \tag{9}$$

where $q_{d(u)} = [(R_N + R_{d(u)})/R_N R_{d(u)}]$, $u_{d(u)} = [(R_N - R_{d(u)})/R_N R_{d(u)}]$, $Q_{d(u)} = (R_F + R_{i3(i1)\uparrow} + R_{i3(i1)\downarrow})q_{d(u)}$, $U_{d(u)} = (R_F + R_{i1(i3)\uparrow} + R_{i1(i3)\downarrow})u_{d(u)}$, $\eta_{N(d,u)} = \exp(-L/\lambda_{N(d,u)})$, $\alpha_{F1(3)} = [(\sigma_{\uparrow1(3)} - \sigma_{\downarrow1(3)})/(\sigma_{\uparrow1(3)} + \sigma_{\downarrow1(3)})]$ [the spin polarization of the conductivity in FM1(3)]. Here, the materials of FM1 and FM3 are the same, and $\alpha_{F1} = \alpha_{F3}$. Under the antiparallel configuration caused by the magnetization reversal of FM3, we replace α_{F3}, $\sigma_{\uparrow3}$, and $R_{i3\uparrow}$ with $-\alpha_{F3}$, $\sigma_{\downarrow3}$ and $R_{i3\downarrow}$ of FM3, respectively. The summation of the electric spin signals and the spin-caloritronic signal from a nondegenerate Si spin valve under the $3T$-MR scheme is quantified as the difference in D under the parallel and antiparallel configurations, and can consequently be described as

$$V_S = D^{\text{parallel}} - D^{\text{antiparallel}} = \left(\frac{\eta_d\left(\frac{1}{R_d} + \frac{1}{R_u}\right)\left[\frac{1}{2}\alpha_{F1}(R_{F1} + R_{i1}) - \frac{(\sigma_{\uparrow1}R_{i1\uparrow} - \sigma_{\downarrow1}R_{i1\downarrow})}{\sigma_{F1}}\right]}{(U_u-1)(U_d-1)\eta_u\eta_d - (Q_d+1)(Q_u+1)}\right)$$
$$\times [(R_{F3}\alpha_{F3} - R_{i3\uparrow} + R_{i3\downarrow})j_e - R_{F3}(\sigma_{\uparrow3}S_{\uparrow3} - \sigma_{\downarrow3}S_{\downarrow3})\nabla T_L], \tag{10}$$

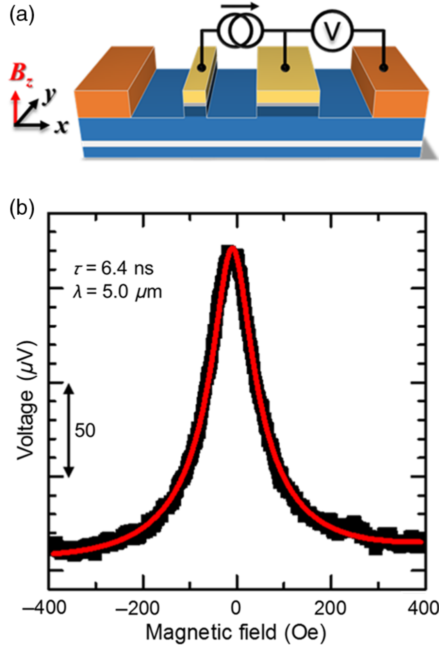

FIG. 3. (a) Experimental setup of the Hanle measurement. The magnetic field is applied parallel to the z axis. (b) The measured Hanle signals (black closed circles) and the theoretical fitting (red solid line) for applied dc current of 3 mA.

where the second term shows the magnitude of the spin-caloritronic signal. We measure the conductivities of Fe and Si at RT to be $\sigma_F = 8.3 \times 10^6$ S m^{-1} and $\sigma_N = 2.12/10^3$ S m^{-1}, and the interface RA is measured to be $2.56/10^{-9}$ Ω m^2 (the spin-injection side, FM2) and 4.66×10^{-9} Ω m^2 (the spin extraction side, FM1). During the measurement, the electric field in the Si spin channel is set to 1.71×10^6 V/m and L is 1.75 μm. λ_N is estimated to be 5.0 μm (accordingly, the spin lifetime is estimated to be 6.4 ns) from the Hanle-type spin-precession experiments in the electric spin-injection scheme as shown in Figs. 3(a) and 3(b), where the magnetic field perpendicular to the plane (parallel to the z axis) is swept. The Hanle-type spin-precession signal is nicely reproduced by the following expression: $(1+\omega^2\tau'^2)^{-0.25}\exp([L/(2\lambda_N)]v\tau' - [L/(\lambda_N)][\sqrt{(\sqrt{1+\omega^2\tau'^2}+1)/2}]\{[\cos(\sqrt{[\arctan(\omega\tau')]^2})/2] + (L/\lambda_N)\sqrt{[(\sqrt{1+\omega^2\tau'^2}-1)/2]}\})$, where D is the spin-diffusion constant, τ is the spin lifetime, $\omega = g\mu_B B/\hbar$ is the Larmor frequency, g is the g factor for the electrons ($g = 2$ in this study), μ_B is the Bohr magneton, $\hbar$ is the Dirac constant, v is the spin-drift velocity, and $\tau' = (v^2/4D) + (1/\tau)$ is the modified spin lifetime by the spin drift. Using values from the literature, we set $\alpha_{F1}(=\alpha_{F3}) = 0.4$ [35], $S = 15$ μV/K at 293 K [36], and $\lambda_F = 9$ nm [37] for Fe at RT. The spin-dependent Seebeck coefficient defined as $S_S = S_\uparrow - S_\downarrow$ is theoretically expressible as $S_S = PS$ [15,38], and the value for Fe is calculated to be 6 μV/K. Thus, the temperature gradient between Fe and Si is estimated to be about 200 mK for a thermal spin signal of 8 μV.

Particular attention is paid to eliminating spurious signals from our estimation of the thermal spin-signal magnitude in silicon. These spurious contributions are due to the nonlinearity of the I-V curves and the bias dependence of the electric spin signals, as described in the experimental part. In this measurement scheme, an rms ac voltage of 1.0 V is applied to the device in addition to a constant bias voltage (3.0 V), and the nonlinearities around the dc bias voltage, 3.0 V, are superposed on the thermal spin signals. We estimate their influence on the basis of experimental data, taking into account the contribution of spurious contribution at 17 Hz. To estimate the spurious signal at 17 Hz, we measure the electrical current as a function of the dc voltage applied in our 3T-MR setup and fit the results to a fifth-order polynomial function: $I = G_1V_{\text{inj}} + G_2V_{\text{inj}}{}^2 + \cdots + G_5V_{\text{inj}}{}^5$ [indicated by the red solid line in Fig. 4(a)], where G_i ($i = 1$–5) is the ith order conductance and V_{inj} is the injection voltage. In the same setup, we also measure the electrical spin signal in a dc configuration as a function of the applied electric current [Fig. 4(b)]. To minimize errors in the fitting and avoid a discrepancy in the fitting curve and the experimental data, wide-range fitting is necessary to corroborate the analysis. (If the signals and fittings are limited within a small bias region, it is difficult to check whether the obtained fitting function can sufficiently reproduce the experimental results.) Thus, these measurements are implemented at the bias voltage of 3.0 ± 1.5 V. We associate this spin signal, denoted by $V_{\text{dc spin signal}}$, to electrical spin injection and spurious effects. We fit these results to a fifth-order polynomial function: $V_{\text{dc spin signal}} = Rs_1I + Rs_2I^2 + \cdots + Rs_5I^5$. By substituting the previous fitted function for I, we obtain $V_{\text{dc spin signal}} = \sum_{i=1}^5 R_{s,i}[\sum_{k=1}^5 G_k(V_{\text{inj}})^k]$, where R_i ($i = 1$–5) is the ith-order resistance. Once we determine the coefficients, we can express the time-dependent contribution as $V_{\text{dc spin signal}}(t) = \sum_{i=1}^5 R_{s,i}\{\sum_{k=1}^5 G_k[V_{\text{inj}}(t)]\}$ under ac + dc excitation, because $V_{\text{inj}}(t) = V_{\text{dc}} + V_0\sin(2\pi ft)$, where f is the ac frequency (17 Hz), V_{dc} is 3.0 V, and V_0 is 1.0 V in this experiment. Through Fourier transformation, the second-harmonic component of $V_{\text{dc spin signal}}(t)$ is calculated. Thus, the time-dependent spectrum and the Fourier transformation spectra of the measured $V_{\text{dc spin signal}}$ are calculated [see Figs. 5(a) and 5(b)]. As shown in Fig. 5(b), the estimated 1f signal is obtained to be 106 μV, which is consistent with the experimental result [ca. 110 μV, see Fig. 4(c)]. On the contrary, the estimated 2f signal is 10.7 μV, inconsistent with the experimental result [ca. 19 μV, shown in Fig. 2(b)]. Note that the calculated 2f signal is not due to the spin-dependent Seebeck effect but due to electrical spin injection and the spurious effects

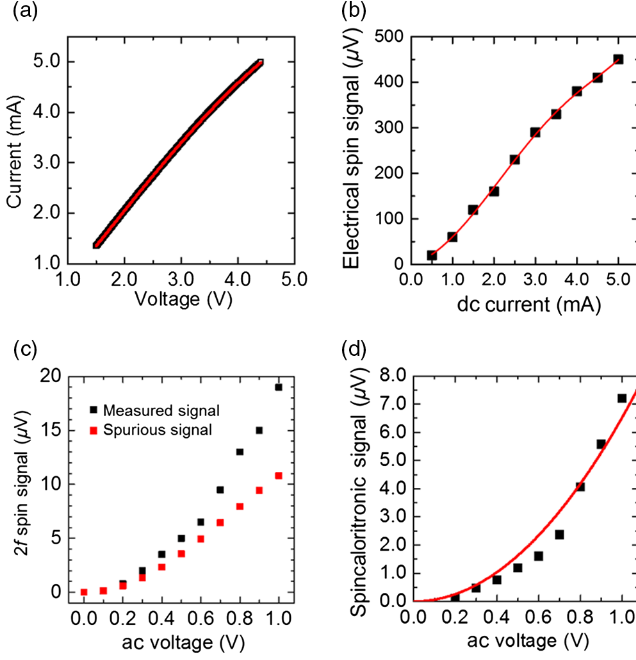

FIG. 4. (a) The bias voltage dependence of the electric current in the nondegenerate Si spin valve at around 3.0 V, the dc offset voltage in the experiment. The black closed squares are experimental results and the red solid line is the fitting curve (the fifth-order polynomial function). (b) The electric current dependence of the electrical spin signal. The black closed squares are experimental results and the red solid line is the fitting curve (the fifth-order polynomial function). (c) Comparison of the measured $2f$ spin signal and the spurious signal that is due to the nonlinearity of the current-voltage curve and the bias current dependence of the electric spin signal. Calculation of magnitude of the spurious signals is described in the main text. The net thermal spin signal is obtained by subtracting the spurious signals from the measured $2f$ spin signal. (d) The net thermal signal as a function of the applied ac voltage with dc offset voltage of 3.0 V. The red solid line is the quadratic fitting function.

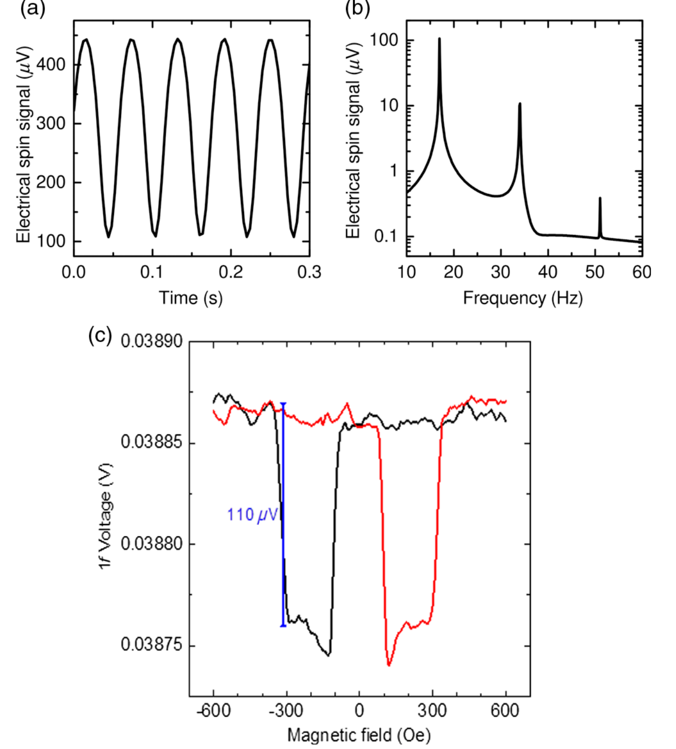

FIG. 5. (a) Time-dependent spectrum of the electric spin signal under the ac (17 Hz) electric current application. (b) A Fourier transformation spectrum of the electric spin signal. (c) The $1f$ spin signal at dc voltage of 3.0 V, ac voltage of 1.0 V, and the ac frequency of 17 Hz.

attributed to the nonlinearity of the $I(V)$ and the bias current dependence of the electric dc spin signals. Hence, the difference of the measured and the calculated $2f$ signal is thus the net thermally generated spin signal.

Figure 4(c) compares the expected second-harmonic components from the spurious effects and the experimental signal obtained using the lock-in method. There is a clear difference between the two signals: 8 μV at an rms ac voltage of 1.0 V, for example. In consequence, the net thermal spin signals are obtained by subtracting the spurious signals from the experimentally measured second-harmonic signals, and they exhibit a quadratic dependence on the rms ac voltage [see Fig. 4(d)], which provides evidence for successful thermal spin-signal detection from a nondegenerate Si spin valve. To note is that the magnitude of the $1f$ signal in this estimation is in good agreement with the magnitude of the $1f$ spin signal obtained experimentally [Fig. 5(b)] and the result of the fifth-order fitting shows the coefficients of the higher-order term becomes monotonically and sufficiently smaller as the order becomes higher as shown in Table I. Both results show our model calculation reproduces the experiments well. It is important in the model to include a contribution of the bias dependence of spin signals, in addition to the nonlinearity of the I-V curve, that has not been considered in similar analyses, although the bias dependence itself is observed in both metal and semiconductor spin valves [34,39] which is ascribed to, for example, the density of states of ferromagnets, heating effects magnon excitation, and so on.

Figures 6(a) and 6(b) show contour plots of the magnitude of thermal spin signals vs conductivity and spin-diffusion length, and vs spin polarization and spin-dependent Seebeck coefficients, respectively. In our calculations, other parameters, such as the thermal gradient,

TABLE I. Coefficients for each order of the polynomial function.

G_1 (A/V)	-2.95×10^{-5}
G_2 (A/V^2)	1.04×10^{-6}
G_3 (A/V^3)	-3.58×10^{-10}
G_4 (A/V^4)	5.80×10^{-14}
G_5 (A/V^5)	-3.84×10^{-18}

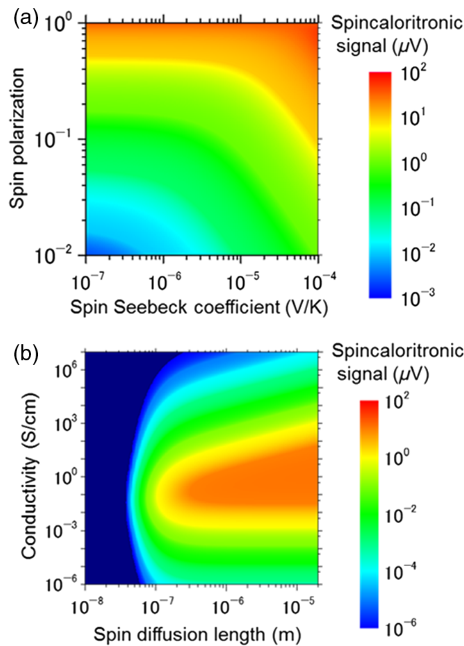

FIG. 6. (a) A contour plot of thermal spin signals due to the spin-dependent Seebeck effect by changing spin polarization and the spin-dependent Seebeck coefficient of the ferromagnet. (b) A contour plot of magnitudes of thermal spin signals due to the spin-dependent Seebeck effect by changing spin-diffusion length and conductivity of a spin channel.

are set to be the same as those used in estimating the thermal gradient of our Si spin devices. Figure 4(a) shows an enhancement in the thermal spin signal due to the spin-dependent Seebeck effect, induced by increasing the spin polarization or spin-dependent Seebeck coefficient of a ferromagnetic electrode. Thus, an introduction of a FM alloy with high spin polarization, such as (Co,Fe)Al [18], with high spin polarization and a large spin-dependent Seebeck coefficient could greatly enhance thermal spin signals. Furthermore, a long spin-diffusion length allows the efficient generation of thermal spin signals [see Fig. 6(b)], because in the case of the spin-dependent Seebeck effect, the heat-induced spin current propagates in a nonmagnetic material and is detected by a detector ferromagnet. Regarding the conductivity, an optimum value for the spin channel conductivity in the thermal spin signal can be seen in Fig. 6(b), which is the manifestation of the conductance mismatch problem [15] as in electrical spin injection in semiconductors [30]. It is notable that a material with metal-like conductivity (approximately $10^6\ \mathrm{S\,m^{-1}}$) cannot generate larger thermal spin signals than a material with lower conductivity (approximately $10^3\ \mathrm{S\,m^{-1}}$). Indeed, semiconductors can generate thermal spin signals that are about 3 orders of magnitude larger, which is a significant advantage of semiconductors.

Finally, let us now discuss the physical difference between the effect observed in our study and other spin-related caloritronic effects. As mentioned above, we use the spin-dependent Seebeck effect [15], which is the spin version of the conventional charge Seebeck effect. The spin Seebeck effect [13,14], the other significant spin-caloritronic effect, arises as a result of the temperature difference between the magnon and electron systems in, respectively, a ferrimagnetic insulator and a heavy metal. The magneto-Seebeck effect [40], which stems from the difference between the charge Seebeck coefficients under parallel and antiparallel magnetization configurations in magnetic tunnel junctions, occurs in the dc component of magnetoresistance. The measurement scheme for the magneto-Seebeck effect is similar to that in this study. However, to note is that the magneto-Seebeck signal appears in the dc component, not in the second-harmonic ac component as in this study, which is the central difference. Thus, the causes of the spin Seebeck and magneto-Seebeck effects are different from that of the spin-dependent Seebeck effect, so the former two effects can be ruled out in our study. "Seebeck spin tunneling" is another effect that can occur in Si [20], and the three-terminal method [21] (not the same as the method we use in this study), which is highly controversial [22–29], was used. Le Breton *et al.* showed that the linewidths and shapes of open-circuit Hanle-like voltage signals in "Seebeck spin tunneling" and "electrical 3*T*" experiments are the same. They claimed that this confirmed successful "spin accumulation" in "Seebeck spin tunneling" experiments. However, one should note that the linewidths of the open-circuit Hanle-like voltages from *n*-type and *p*-type Si in both "Seebeck spin tunneling" and "electrical 3*T*" experiments are the same. The linewidth is governed by the spin lifetime in the channel. (Thus, the lifetime can be estimated by Hanle-effect-related Lorentzian function fitting.) It is well known that in silicon the spin lifetime of electrons in the conduction band is orders of magnitude larger than that of holes in the valence band (since states in the valence band are not pure spin states, and almost any momentum scattering event leads to spin flip) [8,41]. In fact, the spin lifetime of the accumulated spins in *n*-Si (doping concentration, $1.8\times10^{19}\ \mathrm{cm^{-3}}$) using the three-terminal method is reported to be 142 ps at *RT* [21], while the spin lifetime of transported spins in *n*-Si (doping concentration, $5\times10^{19}\ \mathrm{cm^{-3}}$) is estimated to be 1.3 ns by using a nonlocal four-terminal method [41]. The doping concentrations of these two Si devices are almost the same. Furthermore, the Elliot-Yafet spin relaxation takes place in Si, i.e., Si with a lower doping concentration is expected to exhibit a longer spin lifetime. In contrast to the 3*T* method, the nonlocal 4*T* method enables and measures the actual spin transport, and thus, it is one of the most accurate methods to measure spin lifetime. The large discrepancy in the spin lifetime, as measured by the two methods pointed to the nonspin accumulation origin of the signals in the 3*T* method (see also Refs. [22–29] regarding the reliability of the 3*T* signals). Hence, the similarity between the data in Refs. [20,21] shows that the spin lifetime cannot be extracted

using the Hanle-effect-related Lorentzian function in $3T$ experiments, while the origin of this $3T$ open-circuit voltage signal remains unclear [22,23]. In follow-up experiments, other groups using the same $3T$ scheme obtained a similar magnetoresistance not only from semiconductor-ferromagnet tunnel junctions but also from NM-FM junctions, where the spin-orbit strength varies dramatically between different NM metals [24–29]. All of the observed $3T$ open-circuit Hanle-like voltage signals had amplitudes orders of magnitude larger than that of a spin-accumulation signal, and their widths are roughly the same: in contrast to a spin-accumulation signal whose width reflects its spin lifetime. This discrepancy triggered theoretical attempts by a number of groups at understanding the cause of the $3T$ open-circuit voltage signal [26,29]. Their study revealed that this signal arises from spins captured by impurity levels and trap levels in oxide tunneling barriers and/or modulations in the tunneling resistance of oxide barriers induced a magnetic field, and is not related to spin accumulation. The present study demonstrates the spin accumulation and transport in a semiconductor channel (Si) using a spin-caloritronic effect.

IV. SUMMARY

We achieve thermal spin-signal generation in nondegenerate Si by exploiting the spin-dependent Seebeck effect. The thermal gradient at the interface between Fe and Si enables the generation of a spin current in the Si, which is detected as the second-harmonic component of the spin-accumulation voltages at the detector ferromagnet. A simple expansion of the conventional spin-drift-diffusion model that takes into account the spin-dependent Seebeck contribution reproduces the experimental result, and indicates that semiconductor materials are more efficient at heat recycling compared to metallic materials. The present approach is applicable to heat recycling in Si-based devices, such as spin MOSFETs.

ACKNOWLEDGMENTS

This research was supported in part by a Grant-in-Aid for Scientific Research from the Ministry of Education, Culture, Sports, Science and Technology (MEXT) of Japan, Scientific Research(S) "Semiconductor Spincurrentronics" (No. 16H0633). M. S. thanks Dr. F. Rortais for his critical reading of the manuscript and fruitful discussion.

[1] G. E. W. Bauer, E. Saitoh, and B. J. van Wees, Spin caloritronics, Nat. Mater. **11**, 391 (2012).

[2] M. Johnson and R. H. Silsbee, Interfacial Charge-Spin Coupling: Injection and Detection of Spin Magnetization in Metals I, Phys. Rev. Lett. **55**, 1790 (1985).

[3] F. J. Jedema, H. B. Heersche, A. T. Filip, J. J. A. Baselmans, and B. J. van Wees, Electrical detection of spin precession in a metallic mesoscopic spin valve, Nature (London) **416**, 713 (2002).

[4] X. Lou, C. Adelmann, S. A. Crooker, E. S. Garlid, J. Zhang, K. S. Madhukar Reddy, S. D. Flexner, C. J. Palmstrom, and P. A. Crowell, Electrical detection of spin transport in lateral ferromagnet–semiconductor devices, Nat. Phys. **3**, 197 (2007).

[5] T. Sasaki, Y. Ando, M. Kameno, T. Tahara, H. Koike, T. Oikawa, T. Suzuki, and M. Shiraishi, Spin Transport in Nondegenerate Si with a Spin MOSFET Structure at Room Temperature, Phys. Rev. Applied **2**, 034005 (2014).

[6] E. Saitoh, M. Ueda, H. Miyajima, and G. Tatara, Conversion of spin current into charge current at room temperature: Inverse spin-Hall effect, Appl. Phys. Lett. **88**, 182509 (2006).

[7] Y. Kajiwara, K. Harii, S. Takahashi, J. Ohe, K. Uchida, M. Mizuguchi, H. Umezawa, H. Kawai, K. Ando, K. Takanashi, S. Maekawa, and E. Saitoh, Transmission of electrical signals by spin-wave interconversion in a magnetic insulator, Nature (London) **464**, 262 (2010).

[8] E. Shikoh, K. Ando, K. Kubo, E. Saitoh, T. Shinjo, and M. Shiraishi, Spin-Pump-Induced Spin Transport in p-Type Si at Room Temperature, Phys. Rev. Lett. **110**, 127201 (2013).

[9] S. Dushenko, M. Koike, Y. Ando, T. Shinjo, M. Myronov, and M. Shiraishi, Experimental Demonstration of Room-Temperature Spin Transport in n-Type Germanium Epilayers, Phys. Rev. Lett. **114**, 196602 (2015).

[10] R. Ohshima, Y. Ando, K. Matsuzaki, T. Susaki, M. Weiler, S. Klingler, H. Huebl, E. Shikoh, T. Shinjo, S. T. B. Goenenwein, and M. Shiraishi, Strong evidence for d-electron spin transport at room temperature at a $LaAlO_3/SrTiO_3$ interface, Nat. Mater. **16**, 609 (2017).

[11] L. Gravier, S. S. Guisan, F. Reuse, and J.-Ph. Ansermet, Spin-dependent Peltier effect of perpendicular currents in multilayered nanowires, Phys. Rev. B **73**, 052410 (2006).

[12] M. Hatami, G. E. W. Bauer, Q. Zhang, and P. J. Kelly, Thermal Spin-Transfer Torque in Magnetoelectronic Devices, Phys. Rev. Lett. **99**, 066603 (2007).

[13] K. Uchida, S. Takahashi, K. Harii, J. Ieda, W. Koshibae, K. Ando, S. Maekawa, and E. Saitoh, Observation of the spin Seebeck effect, Nature (London) **455**, 778 (2008).

[14] K. Uchida, J. Xiao, H. Adachi, J. Ohe, S. Takahashi, J. Ieda, T. Ota, Y. Kajiwara, H. Umezawa, H. Kawai, G. E. W. Bauer, S. Maekawa, and E. Saitoh, Spin Seebeck insulator, Nat. Mater. **9**, 894 (2010).

[15] A. Slachter, F. L. Bakker, J. P. Adam, and B. J. van Wees, Thermally driven spin injection from a ferromagnet into a non-magnetic metal, Nat. Phys. **6**, 879 (2010).

[16] J. Flipse, F. L. Bakker, A. Slachter, F. K. Dejene, and B. J. van Wees, Direct observation of the spin-dependent Peltier effect, Nat. Nanotechnol. **7**, 166 (2012).

[17] F. K. Dejine, J. Flipse, G. E. W. Bauer, and B. J. van Wees, Spin heat accumulation and spin-dependent temperatures in nanopillar spin valves, Nat. Phys. **9**, 636 (2013).

[18] S. Hu and T. Kimura, Significant modulation of electrical spin accumulation by efficient thermal spin injection, Phys. Rev. B **90**, 134412 (2014).

[19] A. Hojem, D. Wesenberg, and B. L. Zink, Thermal spin injection and interface insensitivity in permalloy/aluminum metallic nonlocal spin valves, Phys. Rev. B **94**, 024426 (2016).

[20] J.-C. Le Breton, S. Sharma, H. Saito, S. Yuasa, and R. Jansen, Thermal spin current from a ferromagnet to silicon by Seebeck spin tunneling, Nature (London) **475**, 82 (2011).

[21] S. P. Dash, S. Sharma, R. S. Patel, M. P. de Jong, and R. Jansen, Electrical creation of spin polarization in silicon at room temperature, Nature (London) **462**, 491 (2009).

[22] Y. Aoki, M. Kameno, Y. Ando, E. Shikoh, Y. Suzuki, T. Shinjo, M. Shiraishi, T. Sasaki, T. Oikawa, and T. Suzuki, Investigation of the inverted Hanle effect in highly doped Si, Phys. Rev. B **86**, 081201(R) (2012).

[23] T. Uemura, K. Kondo, J. Fujisawa, K.-i. Matsuda, and M. Yamamoto, Critical effect of spin-dependent transport in a tunnel barrier on enhanced Hanle-type signals observed in three-terminal geometry, Appl. Phys. Lett. **101**, 132411 (2012).

[24] O. Txoperena, M. Gobbi, A. Bedoya-Pinto, F. Golmar, X. Sun, L. E. Hueso, and F. Casanova, How reliable are Hanle measurements in metals in a three-terminal geometry?, Appl. Phys. Lett. **102**, 192406 (2013).

[25] H. N. Tinkey, P. Li, and I. Appelbaum, Inelastic electron tunneling spectroscopy of local "spin accumulation" devices, Appl. Phys. Lett. **104**, 232410 (2014).

[26] O. Txoperena, Y. Song, L. Qing, M. Gobbi, L. E. Hueso, H. Dery, and F. Casanova, Impurity-Assisted Tunneling Magnetoresistance Under a Weak Magnetic Field, Phys. Rev. Lett. **113**, 146601 (2014).

[27] H. Inoue, A. G. Swartz, N. J. Harmon, T. Tachikawa, Y. Hikita, M. E. Flatte, and H. Y. Hwang, Origin of the Magnetoresistance in Oxide Tunnel Junctions Determined through Electric Polarization Control of the Interface, Phys. Rev. X **5**, 041023 (2015).

[28] O. Txoperena and F. Casanova, Spin injection and local magnetoresistance effects in three-terminal devices, J. Phys. D **49**, 133001 (2016).

[29] I. Appelbaum, H. N. Tinkey, and P. Li, Self-consistent model of spin accumulation magnetoresistance in ferromagnet/insulator/semiconductor tunnel junctions, Phys. Rev. B **90**, 220402(R) (2014).

[30] A. Fert and H. Jaffres, Conditions for efficient spin injection from a ferromagnetic metal into a semiconductor, Phys. Rev. B **64**, 184420 (2001).

[31] Z. G. Yuand M. E. Flatte, Spin diffusion and injection in semiconductor structures: Electric field effects, Phys. Rev. B **66**, 201202(R) (2002).

[32] T. Sasaki, T. Suzuki, Y. Ando, H. Koike, T. Oikawa, Y. Suzuki, and M. Shiraishi, Local magnetoresistance in Fe/MgO/Si lateral spin valve at room temperature, Appl. Phys. Lett. **104**, 052404 (2014).

[33] T. Tahara, Y. Ando, M. Kameno, S. Miwa, Y. Suzuki, H. Koike, T. Sasaki, T. Oikawa, and M. Shiraishi, Observation of large spin accumulation voltages in nondegenerate Si spin devices due to spin drift effect: Experiments and theory, Phys. Rev. B **93**, 214406 (2016).

[34] M. Shiraishi, Y. Honda, E. Shikoh, Y. Suzuki, T. Shinjo, T. Sasaki, T. Oikawa, K. Noguchi, and T. Suzuki, Spin transport properties in silicon in a nonlocal geometry, Phys. Rev. B **83**, 241204(R) (2011).

[35] S. V. Karthink, T. M. Nakatani, A. Rajanikanth, Y. K. Takahashi, and K. Hono, Spin polarization of Co-Fe alloys estimated by point contact Andreev reflection and tunneling magnetoresistance, J. Appl. Phys. **105**, 07C916 (2009).

[36] W. Fulkerson, J. P. Moore, and D. L. McElroy, Comparison of the thermal conductivity, electrical resistivity, and Seebeck coefficient of a high-purity iron and an Armco iron to 1000 °C, J. Appl. Phys. **37**, 2639 (1966).

[37] J. Bass and W. P. Pratt, Jr., Spin-diffusion lengths in metals and alloys, and spin-flipping at metal/metal interfaces: An experimentalist's critical review, J. Phys. Condens. Matter **19**, 183201 (2007).

[38] A. A. Tulapurkar and Y. Suzuki, Contribution of electron-magnon scattering to the spin-dependent Seebeck effect in a ferromagnet, Solid State Commun. **150**, 466 (2010).

[39] S. Valenzuela, D. J. Monsma, C. M. Marcus, V. Narayanamurti, and M. Tinkham, Spin Polarized Tunneling at Finite Bias, Phys. Rev. Lett. **94**, 196601 (2005).

[40] M. Walter, J. Walowski, V. Zbarsky, M. Münzenberg, M. Schäfers, D. Ebke, G. Reiss, A. Thomoas, P. Peretzki, M. Seibt, J. S. Moodera, M. Czerner, M. Bachmann, and C. Heiliger, Seebeck effect in magnetic tunnel junctions, Nat. Mater. **10**, 742 (2011).

[41] T. Suzuki, T. Sasaki, T. Oikawa, M. Shiraishi, Y. Suzuki, and K. Noguchi, Room- temperature electron spin transport in a highly doped Si channel, Appl. Phys. Express **4**, 023003 (2011).